

# Single exciton spectroscopy of semimagnetic quantum dots

J. Fernández-Rossier

*Instituto Universitario de Materiales de Alicante,  
Universidad de Alicante, San Vicente del Raspeig, 03690 Spain*

(Dated: June 26, 2021)

A photo-excited II-VI semiconductor nanocrystal doped with a few Mn spins is considered. The effects of spin-exciton interactions and the resulting multi-spin correlations on the photoluminescence are calculated by numerical diagonalization of the Hamiltonian, including exchange interaction between electrons, holes and Mn spins, as well as spin-orbit interaction. The results provide a unified description of recent experiments of photoluminescence of dots with one and many Mn atoms as well as optically induced ferromagnetism in semimagnetic nanocrystals.

PACS numbers:

Control of the wave function of spins embedded in semiconducting materials is in the road-map of the quantum hardware development<sup>1</sup>. Optical excitation and probing of single exciton confined in a nanometric region permits to manipulate the quantum state of the exciton spin<sup>2,3</sup>, or the spin degrees of freedom coupled to the excitons like nuclei<sup>4</sup>, donor electrons<sup>4,5,6</sup> or Mn ions<sup>5,7,8,9,10,11,12,13,14</sup>. Recent reports<sup>7,8,9</sup> of optical detection of the photoluminescence (PL) of a single nanocrystal of II-VI semiconductor doped with a *single* Mn atom showed evidence of a one on one correspondence between the energy of the emitted photons and the quantum state of the Mn spin after photon emission. Substitutional Mn in (II,Mn)VI semiconductors is a neutral impurity<sup>15</sup> with 5 electrons in the open *d* shell that behave like a spin  $S = \frac{5}{2}$ . Therefore, the experiment of ref. (7) is a proof of principle of the optical manipulation and detection of the quantum state of a single spin  $S = 5/2$ .

Several other groups have reported the fabrication and optical spectroscopy of single nanocrystals of II-VI semiconductors doped with tens of Mn atoms<sup>11,12,13,14,16</sup>. The PL spectrum of one of these semimagnetic nanocrystal is broader than that of a pure dot<sup>7,12</sup>, and it shows strong sensitivity to the application of magnetic fields<sup>12,13</sup>, as a result of the exchange interaction of conduction band (CB) electrons and valence band (VB) holes with the Mn spins. Here, a quantum theory of the single exciton spectroscopy of a nanocrystal with a few Mn spins is presented. The goal is to provide a unified description of the PL spectra of nanocrystals with one<sup>7,8,9</sup> and many Mn atoms, with emphasis on how to extract information about the quantum state of the Mn spins from the PL spectra. With that aim, the standard Hamiltonian for semimagnetic nanocrystals is *solved exactly* for  $N_{Mn} = 1, 2, 3$  and 4 Mn ions both when one exciton is present (excited state manifold, XMS) and absent (ground state manifold, GSM). The optical transition rates between the GSM and XSM are calculated and PL spectra are obtained both in the Faraday and Voigt configurations for a range of situations. Our results agree very well with the PL experiments with dots with one Mn<sup>7,8,9</sup> and many<sup>12,13</sup>. Previous theory work reporting

exact diagonalizations<sup>18,19</sup> have addressed single Mn dots with spherical shape, resulting in PL spectra different from those obtained here and reported experimentally<sup>7,8</sup>.

*Hamiltonian.* The standard Hamiltonian<sup>15,17,18,19,20</sup> for diluted magnetic semiconductors describes CB electrons and VB holes interacting with localized Mn spins ( $\vec{M}_I$ ) via a local exchange interaction and coupling to an external magnetic field,  $\vec{B}$ . For the results presented here the short range antiferromagnetic superexchange is not effective<sup>20</sup>. Both CB electrons and VB holes are confined in all the 3 spacial directions resulting in a discrete single particle spectrum. The Hamiltonian reads  $\mathcal{H} = \mathcal{H}_0 + \mathcal{H}_1 + \mathcal{H}_{eh}$ , where  $\mathcal{H}_0 = -g\mu_B\vec{B} \sum_I \vec{M}_I$  and

$$\mathcal{H}_1 = \sum_{n,\sigma,\sigma'} \left( c_n^e \delta_{\sigma,\sigma'} - g_e \mu_B \vec{B} \cdot \frac{\vec{\tau}_{\sigma,\sigma'}}{2} \right) c_{n,\sigma}^\dagger c_{n,\sigma'} + \sum_\nu \epsilon_\nu^h(\vec{B}) d_\nu^\dagger d_\nu + \sum_I \vec{M}_I \cdot \left( J_e \vec{S}_e(\vec{r}_I) + J_h \vec{S}_h(\vec{r}_I) \right) \quad (1)$$

In the absence of electron-hole (*eh*) pairs, the  $\vec{M}_I$  interact only with  $\vec{B}$ . The first term in  $\mathcal{H}_1$  describes the CB electrons confined in the nanocrystal orbital levels  $\psi_n(\vec{r})$  and coupled to the external magnetic field. The Pauli matrices are denoted by  $\vec{\tau}_{\sigma,\sigma'}$  and  $c_{n,\sigma}^\dagger$  stands for the CB electron creation operator. The second term describes the VB holes confined in the nanocrystal, including the spin orbit interaction<sup>21,22</sup>; the operator  $d_\nu^\dagger$  creates a VB hole in the spin-orbital  $\phi_\nu(\vec{r})$ . The third and fourth term describe the exchange between Mn and CB electrons and VB holes, respectively. Both the CB-Mn and the VB-Mn exchange are local and couple the carrier spin density at the Mn location  $\vec{S}_{e,h}(\vec{r}_I)$  to  $\vec{M}_I$ . The *eh* exchange is described by  $\mathcal{H}_{eh} = -J_{eh} \vec{S}_e \cdot \vec{S}_h$ . Direct *eh* Coulomb interaction and orbital magnetism are irrelevant in the small dots considered here<sup>20</sup>.

We consider dots whose single particle energy spacing is much larger than all the other intra-band energy scales of the Hamiltonian. The shape of the dot determines the degree of light hole (LH) heavy hole (HH) mixing of the VB single particle states which, in turn, determines the relative importance of the Ising and spin flip part of the hole-Mn and hole-electron exchange interactions. A hard

wall cubic potential with dimensions  $L_x, L_y, L_z$  conveniently describes the interplay between the shape of the dot and the single-hole states<sup>21</sup>, although real dots probably have more complicated geometries. We always take  $L_z < L_x, L_y$  and we consider light propagation along the  $z$  axis. The CB electron envelope functions are given by<sup>20</sup>  $\psi_{\vec{n}} \equiv \sqrt{\frac{8}{V}} \text{Sin}(k_x x) \text{Sin}(k_y y) \text{Sin}(k_z z)$  where  $k_i \equiv \frac{\pi n_i}{L_i}$ ,  $i = x, y, z$ ,  $V = L_x L_y L_z$  and  $n_i$  are positive integers. The description of the confined VB single particle states follows that of reference (21): a zero dimensional version of the 6 band Kohn-Luttinger Hamiltonian<sup>22</sup>. The envelope states for the single particle lowest energy doublet are  $|\pm\rangle = c_1 |\frac{3}{2}, \pm\frac{3}{2}\rangle + c_2 |\frac{3}{2}, \mp\frac{1}{2}\rangle$  and  $|-\rangle = \mathcal{K}|+\rangle$  where  $\mathcal{K}$  is the time reversal operation and  $|J, M\rangle$  are the standard<sup>22</sup> light hole (LH) and heavy hole (HH) states at the  $\Gamma_8$  point.

If  $L_x = L_y$  LH-HH mixing vanishes ( $c_2 = 0$ ) and so they do the matrix elements  $\langle \pm | S_h^{x,y} | \mp \rangle$ , resulting in a pure Ising ( $zz$ ) hole-Mn and  $eh$  exchange coupling. For  $0 < |L_x - L_y| < L_z$  there is some HH-LH mixing ( $0 < |c_2| < |c_1|$ ) that, on top of the dominant Ising coupling, permits some spin flip ( $xx, yy$ ) hole-Mn and  $eh$  interaction. In contrast with the VB holes, the CB electron-Mn interaction is perfectly isotropic<sup>20</sup>. The results shown here belong to 4 different dots with  $(L_x, L_y, L_z)$  (7,7,4) nm (dot #1), (15,15,3) nm (dot #2), (7,5,2) nm (dot #3) and (7,3.7,2) (dot #4). The strength of the exchange coupling between the carriers and the Mn spins is  $j_{e,h}(I) \equiv J_{e,h} |\psi_0(\vec{r}_I)|^2$ . For a given dot the mean value of the exchange coupling is  $\langle j_{e,h} \rangle = \frac{J_{e,h}}{V}$  and the maximum value is  $8\langle j_{e,h} \rangle$ . For CdTe we have<sup>15</sup>  $J_h = +60$  meV nm<sup>3</sup> and  $J_e = -15$  meV nm<sup>3</sup>. We take  $g_e = -1.5$  and  $g_h = -0.17$ . In order to establish the influence of the different exchange couplings in the PL spectra of dots with 1 Mn, we first take  $J_{eh} = 0$  (fig. 1) and then we study the effect of  $eh$  exchange (fig. 2a,b,c)

The many body states are classified according to the number of excitons ( $N_X = 0$  for the GSM and  $N_X = 1$  for the XSM) and to the number of Mn ions,  $N_{Mn}$ . The number of states in the GSM of a given nanocrystal is  $(6)^{N_{Mn}}$ . If only the lowest energy doublet of both the CB and VB states are kept, there are four possible exciton states, labeled by  $|\pm 1\rangle_X$  and  $|\pm 2\rangle_X$  following their total angular momentum, and the number of states in the XSM is  $4 \times (6)^{N_{Mn}}$ . The many-body states are found by standard numerical diagonalization of the Schrodinger equations  $\mathcal{H}_0|G\rangle = E_G|G\rangle$  and  $(\mathcal{H}_0 + \mathcal{H}_1)|X\rangle = E_X|X\rangle$ . The GSM states only feature Mn spin coordinates whereas the XSM states include Mn spins, as well as 1 CB electron and 1 VB hole that occupy linear combinations of the single particle states described above.

In the absence of magnetic field and superexchange all the GSM states are degenerate. In contrast, Ising hole-Mn coupling of dot #1 lifts splits the 24 levels in 6 quartets, corresponding to the six possible relative ori-

entations between the Mn and the hole spin along the  $z$  direction. Both electron-Mn and electron-hole exchange coupling further split the 6 quartets into 12 doublets. Depending on the relative size of  $J_{eh}$  and  $J_e$  the lowest energy state of the XSM is either  $|\pm 1\rangle_X \otimes |\mp \frac{5}{2}\rangle$  or  $|\pm 2\rangle_X \otimes |\mp \frac{5}{2}\rangle$ . The diagonalizations show that the lowest energy states of the XSM of dots with  $N_M = 2, 3, 4$  describe fully polarized Mn spins along  $L_z$ . Hence, the exact many-spin wave functions of the Mn coupled to zero dimensional exciton feature ferromagnetic correlations, very much like bulk carrier mediated ferromagnetic order<sup>23</sup> and in agreement with experimental observations in photoexcited nanocrystals<sup>14</sup>.

Transitions from the XSM to the GSM are possible via spontaneous emission of a photon with the adequate energy  $\hbar\omega$  and polarization. We consider circularly polarized photons. The rate of spontaneous emission of a photon of energy  $\hbar\omega = E_X - E_G$  from the state  $|X\rangle$  to the state  $|G\rangle$  is given by the Weisskopf-Wigner expression  $\Gamma_{GX} = \frac{4\omega^3}{4\pi\epsilon_0\hbar c^3} |\langle G | \mathcal{P}^\pm | X \rangle|^2$  where  $\mathcal{P}^\pm = \sum_{\nu, n, \sigma} \langle \nu | e(x \pm iy) | n\sigma \rangle d_\nu^\dagger c_{n,\sigma}^\dagger + \text{h.c.}$  is the second quantization representation of the interband electric dipole operator that yields the standard optical selection rules. Standard optical selection rules forbid photon emission from  $|\pm 2\rangle_X$  states. Since the electric dipole operator does not affect the Mn  $d$  electrons, the Mn spin part of the collective wave function *does not change during the recombination process*. As a result, most of the GSM to XSM transitions that are allowed by the standard optical selection rule but are forbidden due to the orthogonality of the spin part of GSM and the XSM states. This optical spin blockade, reminiscent of the spin blockade well characterized in single electron transport<sup>24</sup>, implies a huge limitation to the otherwise large set of XSM to GSM transitions. The PL spectrum is calculated by statistical weighting of the initial states  $|X\rangle$ :

$$\mathcal{I}_{PL}(\omega) = \sum_{X,G} P(X) \Gamma_{GX} \delta(\hbar\omega - (E_X - E_G))$$

where  $P(X)$  is the occupation probability of the XSM state  $|X\rangle$ . In general the calculation of  $P(X)$  would involve the determination of the non-equilibrium steady state density matrix<sup>17,18</sup>. The experimental results of reference 7 support approximating  $P(X)$  as a thermal distribution function with an effective temperature.

In the following we show PL spectra calculated following the above recipe. The spectral lines are broadened using gaussians with a FWHM of either  $\gamma = 50\mu\text{eV}$  or  $\gamma = 400\mu\text{eV}$ , adapted to the experimental photodetector resolution of references (7) and (12) respectively. Single spin optical spectroscopy calculations are shown in fig. 1. The zero field PL for nanocrystal #1 with a single Mn impurity and 2 effective temperatures, 0.5 and 2 meV (6 and 24 Kelvin) is shown in fig. 1a. The model accounts quantitatively for the experimental observations<sup>7</sup>: only 6 lines are clearly seen, in spite of the fact that the XSM has 12 non degenerate lines, that occupy a spec-

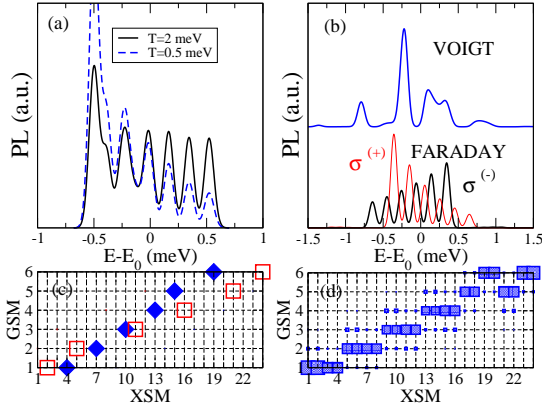


FIG. 1: (Color online). (a) PL for dot #1 with 1 Mn atom and two values of  $T$ . (b) Magneto PL in the Faraday  $((0, 0, 5T))$  and Voigt  $((5T, 0, 0))$  configurations. (c,d)  $\Gamma_{GX}$  for the Faraday (c) and Voigt (d) cases.

tral range of 1 meV. The number of the lines differ from those of previous theory work<sup>(18,19)</sup> due to the different LH-HH mixing of their model. The 6 lines undergo a polarization dependent splitting (fig. 1b, lower spectrum) upon application of a magnetic field in the Faraday configuration,  $\vec{B} = (0, 0, B_z)$ , in good agreement with the experiments<sup>7,10</sup>.

The detection of a photon with a given polarization and energy in one of these 6 peaks yields information about the final state of the GSM in the optical transition. That information is given, for the Faraday spectrum of fig. 1b, in the fig. 1c. There the size of the symbols is proportional to  $\Gamma_{GX}$  for  $\sigma_-$  (open squares) and  $\sigma_+$  (solid diamonds). It is seen how each member of the XSM is coupled via a given circularly polarized photon with, at most, one member of the GSM. This fact *permits to map the photon state (energy and polarization) to the final Mn state* and is the second important result of this paper. In particular, going from low to high energy the six peaks from the PL in the Faraday case correspond to final Mn states going from  $S_z = +\frac{5}{2}$  to  $S_z = -\frac{5}{2}$ . The zero field case has the same one-on-one correspondence.

The calculated PL in the Voigt configuration,  $\vec{B} = (B_x, 0, 0)$ , is remarkably different. The shape of the PL is modified drastically, and the spectrum is much wider. The GSM states are the eigenstates of the  $S_X$  spin operator, whereas the XSM states have strong overlap with the eigenstates of the  $S_z$  operator, because the spin of the hole is pinned in that direction and the hole-Mn Ising coupling is dominant. The matrix  $\langle G|\mathcal{P}|X\rangle$  is now proportional to  $\langle S_x|S_z\rangle$  making spin blockade much less efficient, as shown in fig. 1d. This is seen in figure 1d and accounts for the PL shape reported in 10.

We now consider the effect of the  $eh$  exchange interaction, absent in the results of figure 1. The Ising part of the  $eh$  interaction splits bright and dark excitons, whereas the spin-flip part of the  $eh$  interaction, which is only possible if there is LH-HH mixing, mixes +1 and

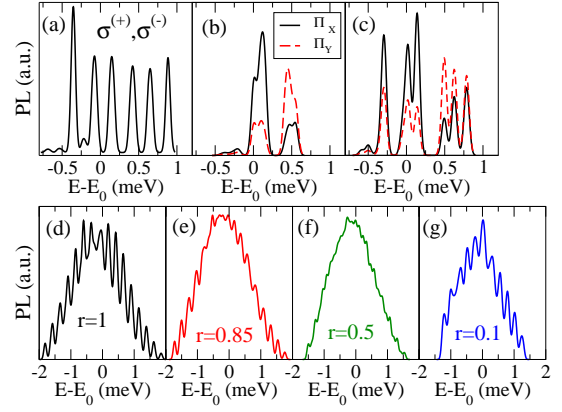


FIG. 2: (Color online). Upper panels: Influence of the LL-HH mixing and the  $eh$  exchange on the PL of single Mn PL for dots #3 (2a) and #4 (2b and 2c). 2d-2g Zero field PL spectrum for dot #2 with 3 Mn impurities as a function of the relative Mn-carrier couplings.

$-1$  excitons resulting into *linearly polarized* spectra<sup>2</sup>. In the presence of Mn, this mixing competes with the Ising hole-Mn coupling. The combined action of electron-Mn exchange and the transverse hole-Mn and  $eh$  interactions mix somewhat bright and dark excitons. In figure 2a-2c we show the PL spectra corresponding to dot #3 (2a) and dot #4 (2b,2c), all of them with a single Mn atom and  $J_{eh} = 1$  meV. Dot #3 features some LH-HH mixing. Ising  $eh$  interaction red shifts the dark excitons, resulting in the appearance of 3 low energy peaks (compared with fig. 1). The middle PL corresponds to a Mn weakly coupled ( $j_h = 0.16$  meV,  $j_e = 0.25j_h$ ) to the exciton and a strong LH-HH mixing. The PL is linearly polarized and the peak structure of figs. 1a is not resolved. The lower panel corresponds to the same dot with a strongly coupled Mn ( $j_h = 0.31$  meV). There the 6 peak structure is recovered, but the PL is linearly polarized, mostly in the central peaks for which the hole-Mn Ising coupling is smaller. This whole picture is consistent and qualitatively identical to the experiments recently published<sup>9</sup>.

We finally address the central theme of this paper: how the PL spectra of the dot evolve as the number of Mn atoms increases. In this regard, we start considering the a dot with 3 Mn atoms, two of which are identically coupled ( $j_h(1) = j_h(2) = 0.38$  meV) and the third changes, so that the relative coupling to the fermions defined by  $r = \frac{|\psi_0(\vec{r}_3)|^2}{|\psi_0(\vec{r}_{1,2})|^2}$  is varied from 1 to 0.1 (figs 2d to 2g). The symmetric case  $r = 1$  shows a clean PL spectrum with 16 lines corresponding to quantum states with the  $2S+1$  possible orientations of the collective  $S_Z$  of the 3 Mn atoms that behave like a single magnet with  $(S = 15/2)$ . These 16 peaks are still seen for  $r = 0.85$ . At  $r = 0.5$  the PL is a rather featureless wide peak. When  $r = 0.1$  the PL spectrum features 11 peaks, that are the analog of figure 2d for 2 Mn atoms behaving collectively with  $S = 10/2$ . It is apparent that the weakly coupled Mn spin does not affect the PL.

The results of figure 2d-2g suggest that a few Mn atoms, strongly coupled to the exciton could be responsible of the main features of the PL signal observed in earlier experiments. In ref. (12) the PL spectrum of single semimagnetic nanocrystals show a zero field  $\sigma^+$  line with a full width at half maximum (FWHM) of  $\simeq 5$  meV that red shifts and narrows upon application of a magnetic field in the Faraday configuration<sup>11,12,13</sup>. This has motivated statistical interpretation of the PL spectrum of single semimagnetic nanocrystals<sup>12,13</sup>, linking the PL linewidth to the magnetic statistical fluctuations. In such an approach the PL FWHM has been shown to scale with  $\sqrt{\frac{k_B T}{V}}$ . On the other side, it is apparent that the PL spectrum of a single Mn impurity<sup>7</sup> lies in a window of order  $\Delta_I = \frac{5}{2} (|j_h(I)| + |j_e(I)|)$ , which scales like  $V^{-1}$ . The PL linewidth of fig. 2 also scales with  $\sum_I \Delta_I \propto V^{-1}$ .

We have explored whether the quantum approach with  $N_{Mn}=3$  and 4 can model PL spectra like those of references (11,12,13). The justification lies in the distribution of couplings  $j_h(I)$ , shown in fig. 3a for Cd<sub>0.99</sub>Mn<sub>0.01</sub>Te (dot #1) obtained by random generation of 100 realizations of the Mn disorder. Such a dot has  $N_{Mn}=28$  and  $\langle j_h \rangle = 0.3$  meV. However, 65 % of the Mn have  $j_h < \langle j_h \rangle$  and, in average, the 4 Mn with largest coupling have  $j_h > 3\langle j_h \rangle$ . We calculate the PL taking the 4 Mn atoms with the largest overlap to the carrier wave function, for a randomly selected Mn disorder realization. Their  $j_h$  are 1.69, 1.66, 1.1, and 0.45 meV. In figure 3b we show the corresponding  $\sigma^+$  PL spectrum for values of the magnetic field going from zero to 12 T in the Faraday configuration. We take  $\gamma = 0.4$  meV and  $T = 3$  meV. As in the experiments, the  $\sigma^+$  PL red shifts as  $B_z$  goes up. The featureless zero field PL spectrum (with a FWHM of 5 meV) develops, as  $B_z$  increases narrow structures, as reported experimentally<sup>13</sup>. The narrowing is also seen in fig. 3c, that shows the PL of dot #1 with 3 Mn atoms, with values of  $j_h$  closer to the average (0.39, 0.40 and 0.44 meV), with  $T = 2$  meV and  $\gamma = 0.4$  meV. In fig. 3d we show how the corresponding FWHM decreases both upon cooling and upon increasing  $B_z$ . The former is due to the reduction of the spectral range of the occupied states in the XSM, resulting as well in a red shift that has been observed experimentally<sup>12</sup>. The magnetic field produces a similar effect.

In conclusion, the problem of a few Mn atoms interacting with a single exciton in a quantum dot is solved

via numerical diagonalization of the Hamiltonian including electron-Mn, hole-Mn, electron-hole exchange as well as spin-orbit interactions and the corresponding PL spectra are calculated. The model accounts for a series of recent reports with the PL of CdTe dots doped with a single Mn atom and permits to link the quantum state of one Mn spin to the detection of a photon with a given energy and polarization. The crucial ingredient for this one on one correspondence is the anisotropy of the hole-Mn interaction, due to strong spin-orbit interaction for the holes. The model reproduce qualitatively the PL spectra of single dots with presumably tens of Mn atoms<sup>11,12,13</sup> with just 3 and 4 Mn spins strongly coupled to the exciton and with different coupling strengths. This might indicate that the width of the PL spectra coming from a single semimagnetic dot might arise from a few Mn atoms strongly coupled to the exciton rather than from statistical fluctuations of many Mn atoms.

L. Besombes and H. Mariette are acknowledged for sharing their data before publication. Fruitful discussions with J. J. Palacios and funding from Grant FIS200402356 and the Ramon y Cajal Program (MEC, Spain) are acknowledged. This work has been partly funded by FEDER funds.

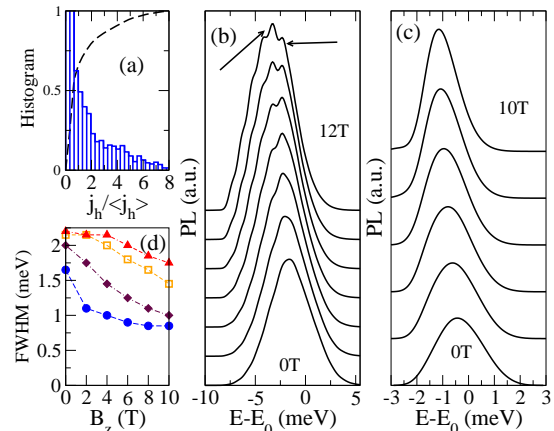


FIG. 3: (Color online). (a) Normalized histogram of Mn-hole coupling. The dashed line is the integrated histogram. (b) PL spectrum for 4 Mn impurities (see text) for several values of  $B_z$ . (c) Idem for 3 Mn impurities. (d) FWHM for as a function of  $B_z$  and  $T=3,2,1$  and 0.5 meV (top to bottom).

<sup>1</sup> B. E. Kane, Nature (London), 393, 133 (1998). D. Loss *et al.*, Phys. Rev. A **57**, 120 (1998).  
<sup>2</sup> N. H. Bonadeo *et al.*, Science **282**,1473 (1998)  
<sup>3</sup> Xiaoqin Li *et al.* Science **301**, 809 (2003).  
<sup>4</sup> F. Jelezko *et al.*, Phys. Rev. Lett. **93**, 130501 (2004)  
<sup>5</sup> J. Bao, *et al.*, Nature Mater. **2**, 175 (2003).  
<sup>6</sup> P. Chen *et al.*, Phys. Rev. B **69**, 075230 (2004)  
<sup>7</sup> L. Besombes *et al.* Phys. Rev. Lett. **93**, 207403 (2004)

<sup>8</sup> L. Besombes *et al.* Phys. Rev. B. **71**, 161307 (2005)  
<sup>9</sup> Y. Léger *et al.*, Phys. Rev. Lett. **95**,047403 (2005)  
<sup>10</sup> Y. Léger *et al.*, submitted to PRB  
<sup>11</sup> A. A. Maksimov *et al.* Phys. Rev. B **62**, R7767 (2000)  
<sup>12</sup> G. Bacher *et al.*, Phys. Rev. Lett. **89**, 127201 (2002)  
<sup>13</sup> P. S. Dorozhkin *et al.*, Phys. Rev. B **68**, 195313 (2003)  
<sup>14</sup> S. Mackowski *et al.* Appl. Phys. Lett. **84**, 3337 (2004).  
<sup>15</sup> J. K. Furdyna, J. Appl. Phys **64** R29 (1988).

- <sup>16</sup> S. C. Erwin *et al.*, Nature **436**, 91 (2005)
- <sup>17</sup> A. Efros, E. Rashba, M. Rosen, Phys. Rev. Lett. **87**, 206601 (2001)
- <sup>18</sup> A. O. Govorov, Phys. Rev. B **70**, 035321 (2004) A. O. Govorov and A. V. Kalameitsev Phys. Rev. B **71**, 035338 (2005)
- <sup>19</sup> A. K. Bhattacharjee and J. Pérez-Conde Phys. Rev. B **68**, 045303 (2003)
- <sup>20</sup> J. Fernández-Rossier and L. Brey, Phys. Rev. Lett. **93** 117201 (2004)
- <sup>21</sup> F. V. Kyrychenko and J. Kossut, Phys. Rev. B **70**, 205317 (2004)
- <sup>22</sup> J.M. Luttinger, W. Kohn, Phys. Rev. **97** 869 (1955)
- <sup>23</sup> H. Ohno, Science **281**, 951 (1998). T. Dietl *et al.*, Science **287** 1019 (2000).
- <sup>24</sup> J. J. Palacios *et al.*, Phys. Rev. B **50** 5760 (1994)